IOP Conf. Series: Materials Science and Engineering **377** (2018) 012090 doi:10.1088/1757-899X/377/1/012090

Turbulent Flow Characterization over the Gravel Bed

Abhranil Adak[1]

[1]Assistant Professor, Department of Civil Engineering, Sikkim Manipal Institute of Technology, Sikkim Manipal University, Rangpo, Majitar, Sikkim-737132.
Email: abhranil2001@gmail.com

Abstract: The double-averaged momentum equations are used as a natural basis for the hydraulics of rough-bed open channel flows, especially with small relative submergence. To study the double-averaged turbulence characteristics in flows over a gravel-bed, a uniform flow over a gravel-bed was run in a laboratory flume and the velocities were measured at different verticals by a vectrino probe. The result reveals that the local time-averaged velocity profiles can be split into three typical classes, namely log, S-shaped and accelerated. In the log class velocity profile fits a logarithmic curve over almost the entire measured profile. S Shaped refers to profiles that can be encountered in wake of macro-roughness bed elements due to flow separation on the lee side. The accelerated profile located in the vicinity of top of the macro-roughness elements and the velocities are slightly higher than log classes but rapidly drop to zero below crest. It never extends to zero bed level above the crest they are not influenced by the bed heterogeneity. The logarithmic law of velocity profile is preserved above the roughness crest and velocity below the crest follows a polynomial. The field of gravel-bed appears to be near Gaussian matches with the work of previous researchers. The Reynolds shear stress is the main governing stress across the flow depth with a damping in the vicinity of gravel bed due to decrease in turbulence level. The form induced stress is prominent below the roughness crest.

Keywords: Local flow characteristics; Spatial-averaging; Turbulent flow

1. Introduction

Turbulent flow in open-channel with hydraulically smooth beds has been significantly clarified in the last few decades. The near-bed flow structure in deep flows over irregular rough beds is still unclear in many and they provide valuable knowledge for time-averaged turbulent flow characteristics over gravel bed. In the gravel-bed streams, the turbulent flow characteristics are strongly influenced by the heterogeneity of bed topography comprised of discrete particle of various shapes and orientations. The time averaged flow structure is highly 3D and spatially heterogeneous near irregular rough beds, which makes the time-averaged momentum equations inconvenient and impracticable [8] [14] [15] [16]. Therefore the time averaging of Navier-Stoke equations supplemented by spatial area (or volume) averaging in the plane parallel to the averaged bed. It explicitly defines important additional term such as form-induced stress and form drag [16]. These double averaged variables can be applied even for the flow region below roughness crests and make it possible to have an insight to the hydrodynamics within the flow sub-layers induced by rough elements. These sub layers are form-induced and interfacial sub-layer, which are together called roughness sub-layer. The form-induced sub- layer occupies the flow zone just above the roughness crests is influenced by individual roughness elements. The concept of spatial averaging was first introduced by Smith and McLean [1] [8] in hydraulics for considering vertical velocity profiles along lines of constant distance from a wavy bed and by Wilson and Shaw [2] for describing atmospheric

flows within vegetation canopies. Further contributions were made by Raupach and Shaw [4], Finnigan [5], and Raupach *et al.*[6] [7] to enable the flow to be averaged over any volume within the canopy which is known as volume-averaging concept. Gimenez-Curto and Corniero Lera (1996) also successfully applied a similar approach to describe oscillating turbulent flows over very rough surfaces. Although the idea of spatial averaging has been used by many researchers [8] [9] [10] the full development of this approach to use in hydraulics was fully made by Nikora *et al.*[18] [19], who developed new continuity and momentum equations for rough-bed open channel flows by double-averaging the Navier-Stokes equations.

2. Spatially Averaged Navier Stokes Equation

The averaging procedure for area averaging at a level z is defined as [3]

$$\langle\theta\rangle(x,y,z,t)=\frac{1}{A_f}\iint_{A_f}\theta(x',y',z,t)\,dx'dy'$$

Where θ is the flow variable defined in the fluid to be spatially averaged over the fluid domain A_f = area occupied by fluid within a fixed region on the *x, y* plane at elevation z with total area A_0; and angle brackets denote spatial averaging.; (*x*, *y*, *z*, *t*) is the space and time coordinate oriented along main flow parallel to average bed level; $x'$and y' are the fluctuations of x and y;. It is the right-handed coordinate system, x axis is oriented along the main flow parallel to the averaged bed (u = velocity component), y-axis is oriented to the left bank (v = velocity component), and z axis is pointing towards the water surface (w = velocity component). The total area includes the domain occupied by the fluid and intervening solid surfaces. Below roughness crests the averaging region is multiply connected, since it is intersected by roughness elements. The square root of the area A_0 may be interpreted as a scale of a spatial rectangular window smoothing irregularities with a linear scale $< A_0^{0.5}$.

The conventional Reynolds equations are:

$$\frac{\partial\overline{u}_i}{\partial t}+\overline{u}_i\frac{\partial\overline{u}_j}{\partial x_i}=g_i-\frac{1}{\rho}\frac{\partial\overline{p}}{\partial x_i}-\frac{\partial\overline{u_i'u_j'}}{\partial x_j}+\nu\frac{\partial^2\overline{u}_i}{\partial x_j^{\,2}} \qquad (1)$$

$$\frac{\partial\overline{u}_i}{\partial x_i}=0$$

Applying the basic equation in the above equations, one gets the spatial-averaged equations for the flow regions above and below the roughness elements.

Flow region above the crests of roughness elements $z > z_c$:

$$\frac{\partial\langle\overline{u}_i\rangle}{\partial t}+\langle\overline{u}_i\rangle\frac{\partial\langle\overline{u}_j\rangle}{\partial x_i}=g_i-\frac{1}{\rho}\frac{\partial\langle\overline{p}\rangle}{\partial x_i}-\frac{\partial\left\langle\overline{u_i'u_j'}\right\rangle}{\partial x_j}-\frac{\partial\left\langle u_i'u'_j\right\rangle}{\partial x_j}+\upsilon\frac{\partial^2\left\langle\overline{u_i'}\right\rangle}{\partial x^2{}_j} \qquad (2)$$

$$\frac{\partial \langle \overline{u}_i \rangle}{\partial x_i} = 0$$

Flow region below the crests of roughness elements $z < z_c$:

$$\frac{\partial \langle \overline{u}_i \rangle}{\partial t} + \langle \overline{u}_i \rangle \frac{\partial \langle \overline{u}_j \rangle}{\partial x_i} = g_i - \frac{1}{\rho}\frac{\partial \langle \overline{p} \rangle}{\partial x_i} - \frac{1}{\phi}\frac{\partial \phi \left\langle \overline{u_i' u_j'} \right\rangle}{\partial x_j} - \frac{1}{\phi}\frac{\partial \phi \left\langle u_i' u'_j \right\rangle}{\partial x_j} + \upsilon \frac{\partial^2 \left\langle \overline{u_i'} \right\rangle}{\partial x^2{}_j} + \nu \left\langle \frac{\partial^2 \tilde{u}_i}{\partial x^2{}_j} \right\rangle - \frac{1}{\rho}\frac{\partial \langle \tilde{p} \rangle}{\partial x_i} \quad (3)$$

$$\frac{\partial \phi \left\langle \overline{u_i} \right\rangle}{\partial x_i} = 0$$

where z_c = elevation of the highest roughness crests; In the above equations the straight overbar and angle brackets denote the time and spatial average of flow variables, respectively; the wavy overbar ($\tilde{\theta}$) denotes the spatial fluctuation in the time-averaged flow variables, i.e., the difference between time averaged flow quantity $\overline{\theta}$ and spatially-averaged quantities $\langle \overline{\theta} \rangle$. and ϕ = roughness geometry function, A_f/A_0. Tensor notations are used here for velocity subscripts. Equations describe relations between spatially averaged flow properties and contain some additional terms in comparison with basic equation. These terms are form-induced stresses, form drag, and viscous drag on the bed. The form-induced stress $\left\langle \tilde{u}_i \tilde{u}_j \right\rangle$, form drag $(1/\rho)$ $\left\langle \partial \tilde{p} / \partial x_i \right\rangle$ and viscous drag $\upsilon \left\langle \partial^2 \tilde{u}_i / \partial x_j{}^2 \right\rangle$ appear as a result of spatial averaging.

At high Reynolds numbers viscous stress is negligible everywhere except in the vicinity of the wall and therefore equations can be reduced to give the momentum equations

Flow region above the roughness crests:

$$gS - \frac{\partial \langle \overline{u'w'} \rangle}{\partial z} - \frac{\partial \langle \tilde{u}\tilde{w} \rangle}{\partial z} = 0$$

$$g\cos\alpha + \frac{1}{\rho}\frac{\partial \langle \overline{p} \rangle}{\partial z} + \frac{\partial \langle \overline{w'^2} \rangle}{\partial z} + \frac{\partial \langle \tilde{w}^2 \rangle}{\partial z} = 0 \quad (4)$$

Flow region below the roughness crest:

$$gS - \frac{1}{\rho}\left\langle \frac{\partial \tilde{p}}{\partial x} \right\rangle - \frac{1}{\phi}\frac{\partial \phi \langle \overline{u'w'} \rangle}{\partial z} - \frac{1}{\phi}\frac{\partial \phi \langle \tilde{u}\tilde{w} \rangle}{\partial z} = 0 \quad (5)$$

$$g\cos\alpha+\frac{1}{\rho}\frac{\partial\langle\overline{p}\rangle}{\partial z}+\frac{1}{\rho}\left\langle\frac{\partial\tilde{p}}{\partial z}\right\rangle+\frac{1}{\phi}\frac{\partial\phi\langle\overline{w'^2}\rangle}{\partial z}+\frac{1}{\phi}\frac{\partial\phi\langle\tilde{w}^2\rangle}{\partial z}=0 \qquad (6)$$

These equations represent the spatially-averaged momentum equations are for the longitudinal velocity component and the spatially-averaged momentum equations in the vertical domain.

3. Experimentation

Experiments over gravel-bed were conducted in a 0.9 m wide, 0.75 m deep and 15 m long horizontal flume. At the test section, the sidewalls of the flume were made of 2.0 m long transparent glasses. The test section was located 8 m from the upstream end of the flume. Uniform gravel of d_{50} equaling 40 mm was laid over the flume bottom to simulate the turbulent flow over the gravel bed. The gravel bed was prepared homogeneously spreading uniform gravel in four layers to create the random variation of bed surface. The bed surface elevation was measured every 1 m interval. For the characterization of bed the bed elevation was measured 5 mm interval from 8 to 9.5 m by vernier point gauge with a precession of ±0.1 mm. In order to achieve a uniform flow condition the flow depth was controlled adjustable tailgate at the downstream end of the flume. Point gauges were placed at 1.0 m interval along the centerline of the flume. The experiment was run for a flow depth of 0.19 m. Flow uniformity was checked by the measuring the free water surface slope. Velocity measurements were captured at 50 horizontal locations at 20 mm interval. The measuring zone was sufficiently away from the tailgate in order to avoid downstream boundary conditions.

4. Results

On gravel-bed roughness characterization there are two classical approaches [11] [12]. They are characteristic particle size approach and random field approach. The first approach is that the surface of gravel bed is composed of discrete particles forming bed roughness. In the second approach the bed surface is the random field of elevations. The bed roughness is to consider it as a random field of bed elevations $Z(x, y. t)$ (the origin of Z is lower than channel bed surface, at an arbitrary level), where x and y are the longitudinal (the main flow direction) and the transverse coordinates and t is time. In the experiment it is observed that the field of gravel-bed elevations appears to be near Gaussian. This has given us a reason to apply the second-ordered structure function for describing gravel bed roughness.

The Nikuradse's equivalent sand roughness k_s is the standard deviation of bed surface profile 8.053 mm. The height of crest above mean bed level is 14.4128 mm and the depth of lowest level below mean bed level is 21.287 mm.

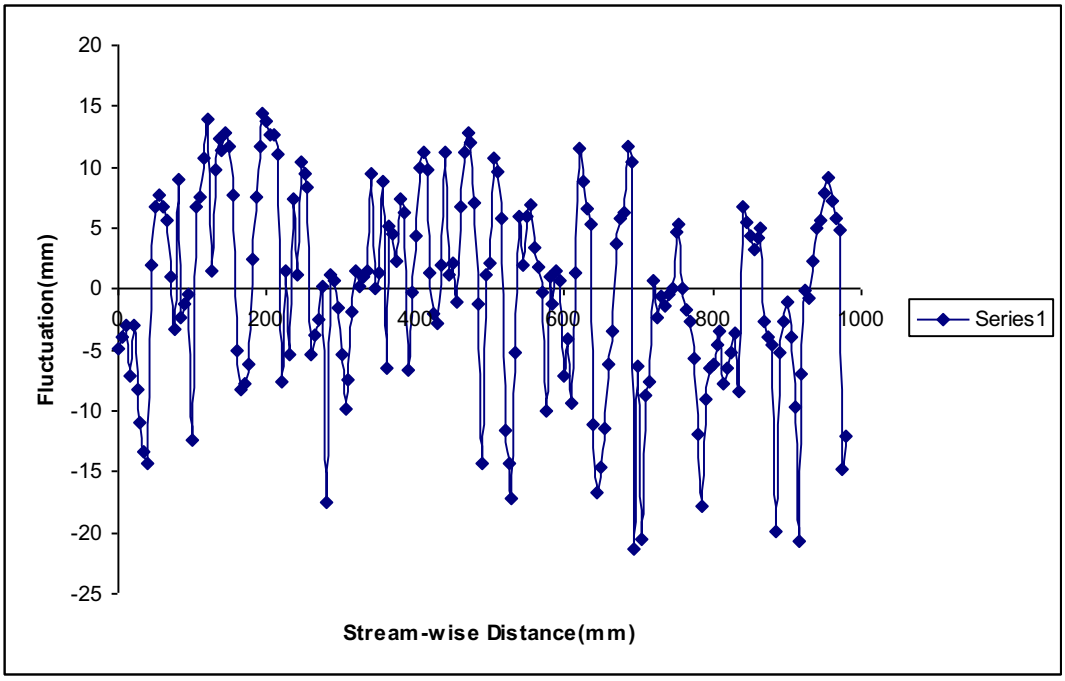

Fig 1: Bed Surface Profile

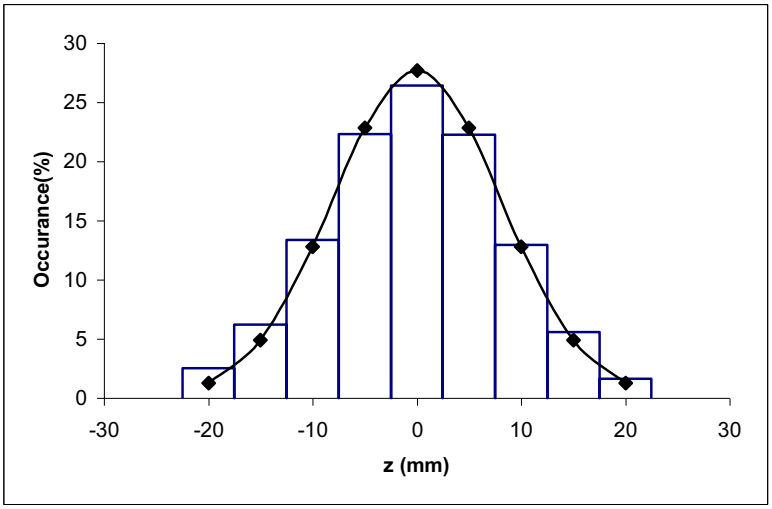

Fig 2: Bed Elevation Distribution

Fig. 3 shows the variation of ϕ with z obtained from the measurement of the bed surface elevations by a point gauge. It is pertinent to mention that the estimation of estimation of ϕ-function, reported by Aberle [1], using the point gauge data, was only suitable for the upper

70% of the interfacial sub-layer, although a carefulness could make achieving the estimation quite acceptable Mignot *et al.*[12] [13]

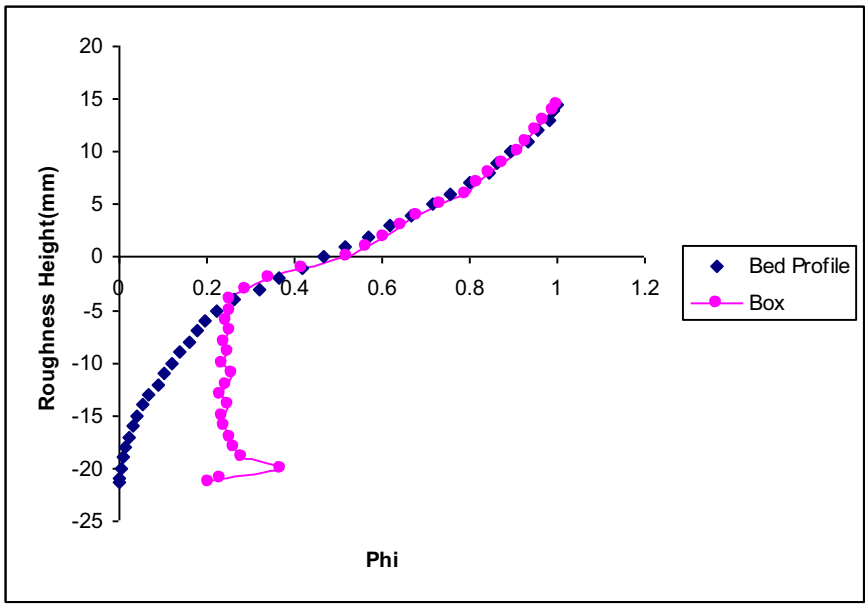

Fig 3: Variation of Roughness Geometry Function ϕ with z

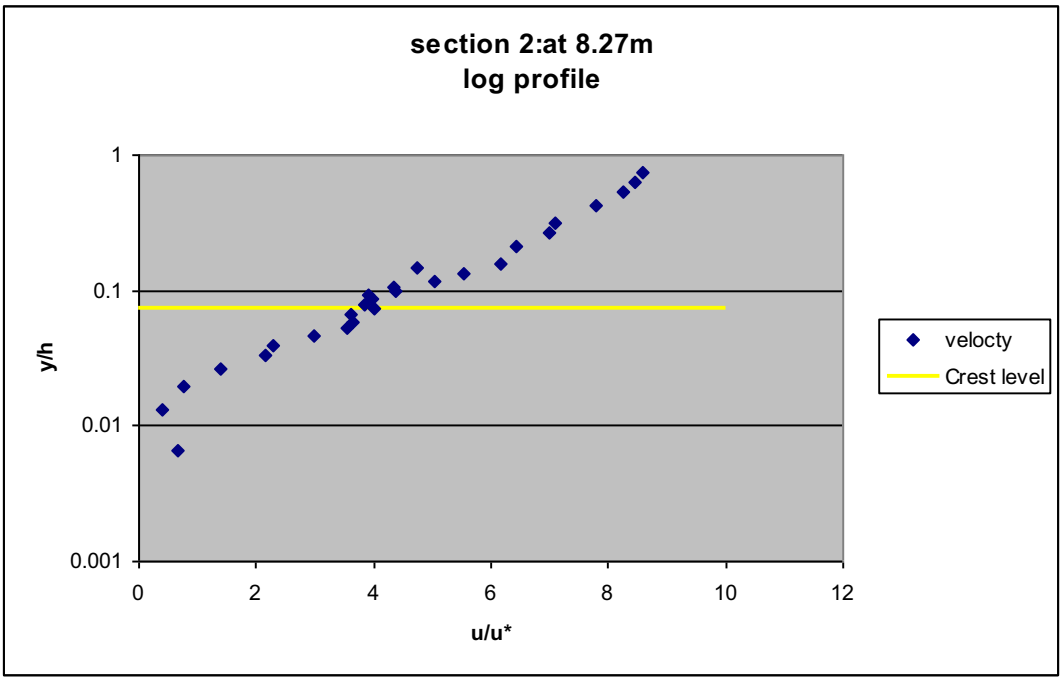

Fig 4: Logarithmic Velocity Profile

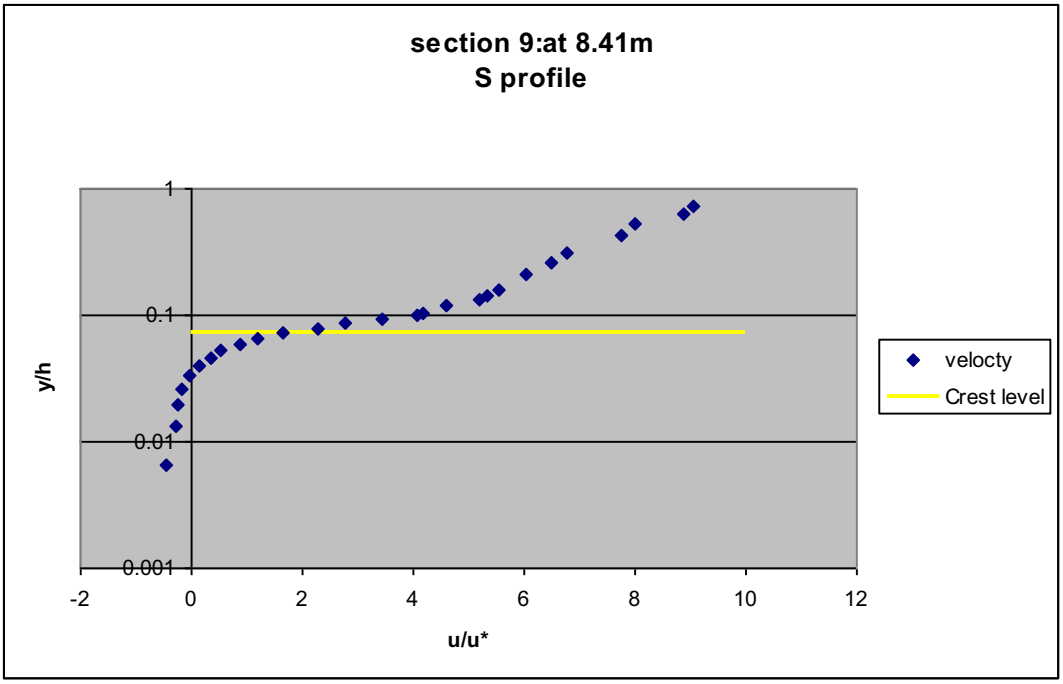

Fig 5: S-Shaped Velocity Profile

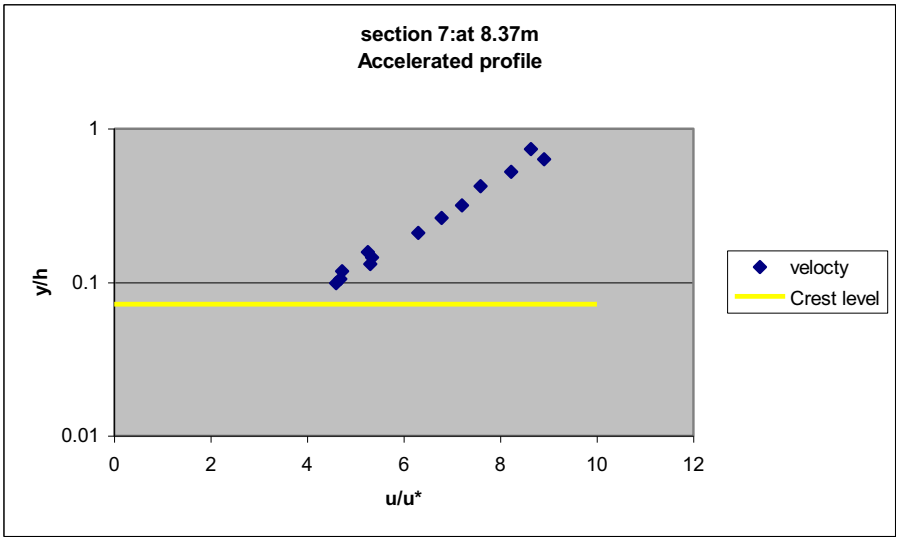

Fig 6: Accelerated Velocity Profile

The local characterization of the flow is associated with the double-averaged one. Hoover & Ackerman proposed a classification of the flow characteristics in different classes, depending on the properties of the local time-averaged velocity profiles. They suggested defining three classes of velocity profiles around individual macro-roughness bed elements with very low relative submergence: the 'logarithmically distributed', the 'S-shaped' and the 'wedge-shaped' profiles. Similar tendencies were also reported for higher relative submergences.

For the log profile in Fig. 4 the mean streamwise velocity fits a logarithmic curve over almost the entire measured profile. The second class called S-Shaped refers to profiles that can be encountered in the wake of macro-roughness bed elements due to flow separation on the lee side. These particularly important velocity profile exhibit an inflexional behavior specific to retarded flows as in confined detached flows that are also very similar to mixing layer
In the accelerated profiles (Similar to the wedge-shaped profiles defined by consist of profiles located in the vicinity of the top of the macro-roughness elements. The associated velocities are slightly higher than the log class ones above z_c and rapidly drop to zero at or slightly below the top of the highest roughness element.
It is observed that above the crest level they are not influenced the bed heterogeneity, all classes behave quite similar. Below crest level they differ significantly. Of the 50 profiles the following class distribution was obtained: 28 are log profiles; 14 are S- shaped profiles; 8 are accelerated profiles.
In the Fig.7 three different types of velocity profiles are shown along with roughness geometry function and without roughness geometry function. Fig. 8 shows the plot of three typical profiles of each class and the streamwise locations of the 50 equally spaced profiles above the gravel-fluid interface topography along with the labels indicating their class. The spatial distribution of the labels is obviously closely related to the location with regard to the macro roughness bed elements. In the zones with local bed gradients (x – 8.43 to 8.63) all the profiles belong to the log class. In contrast, close to the top and downstream from the highest gravel elements the profiles belong to the accelerated and S-shaped classes, respectively. They confirm the trend observed by Hoover & Ackerman in the vicinity of single macro-roughness bed elements.

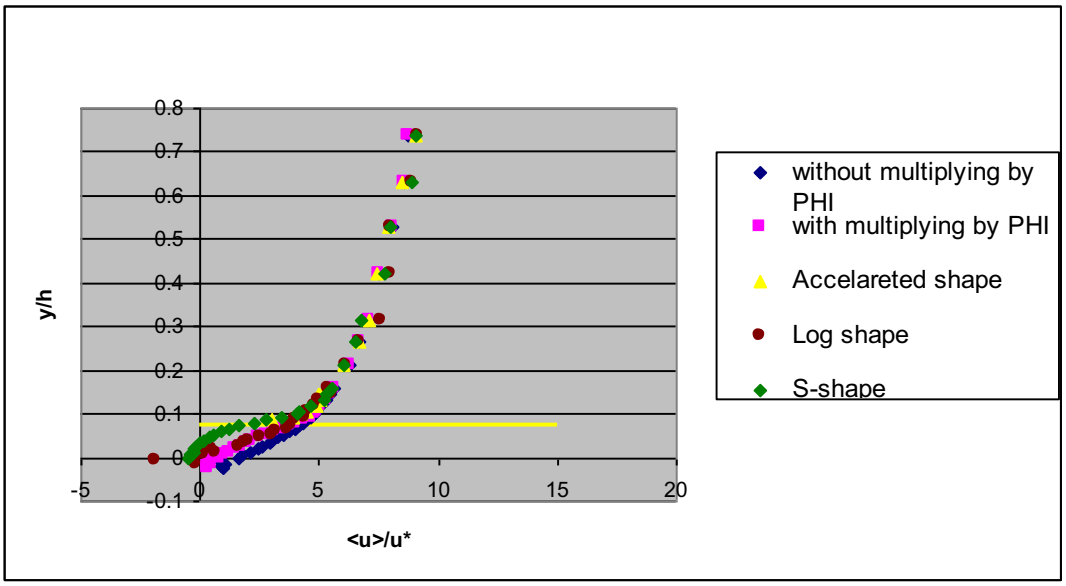

Fig 7: Examples of local profiles of time-averaged streamwise velocity chosen in each of three classe

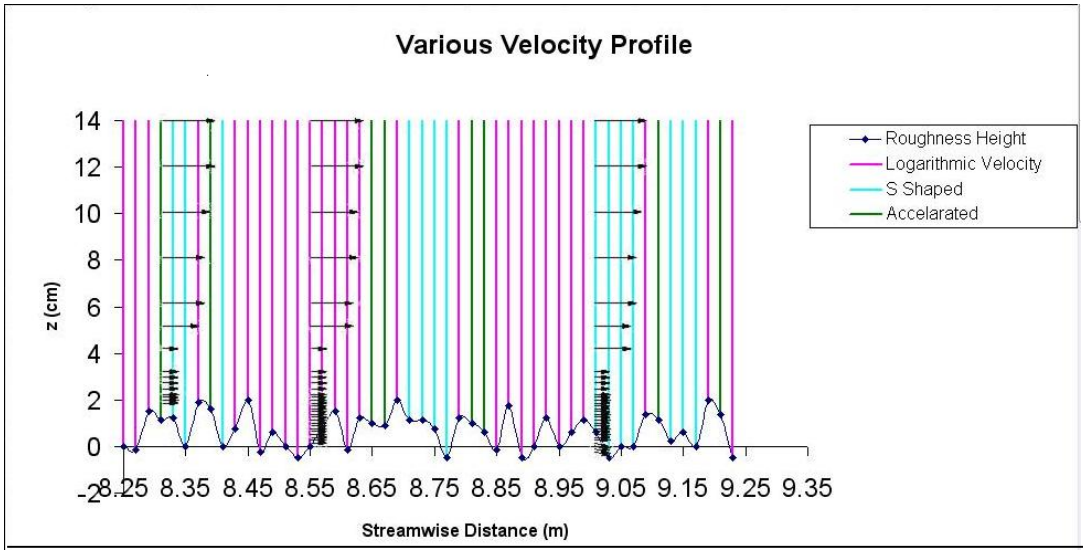

Fig 8: Local mean streamwise velocity from ADV measurement and bed topography

Red line log profile, Green line accelerated profile and Sky blue line S Shaped profile

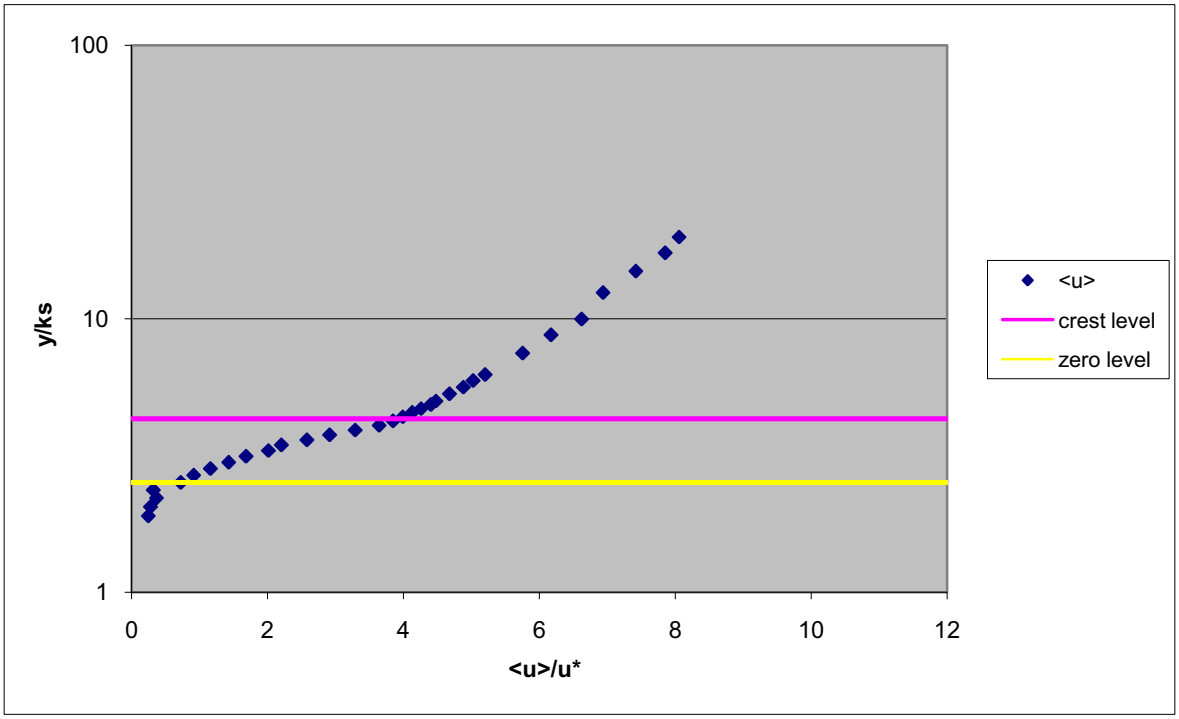

Fig 9: Vertical Distribution of normalised DA streamwise velocity

Figure 9 depicts the variation of normalized SA streamwise velocity $\langle u^+ \rangle$ (= $\langle \bar{u} \rangle / u_*$) with z/k_s, The SA $\bar{u}$ (and also other turbulence quantities) at a distance z was obtained from 50 superficial measuring points. In the 5 measurements we reach below mean bed level. In 42 measurements where $z < z_c$ with multiplying with roughness geometry function $\langle \bar{u} \rangle$ is obtained. The shear velocity u_* [= $(\tau_0/\rho)^{0.5}$; in which τ_0 is the bed shear stress] equaling 0.066 m/s that is used to scale the flow and turbulence quantities, is determined from the Reynolds shear stress profile extending the linear profile on the top level of the interfacial sub-layer (that is the crest level of the gravels), that is $u_* = (-\overline{u'w'})^{0.5}\Big|_{z=z_c}$, in which u' and w' are the fluctuations of streamwise and vertical velocities, respectively. The value of u_* obtained from the bed slope is 0.061 m/s that is close to that of u_* obtained from the Reynolds shear stress profile. It is observed that the velocity profile above the crest follows the logarithmic law where below crest follow polynomial. It is in conformity with Bose and Dey [5] [6] that inner- and outer-layers of fluid flow correspond to a polynomial and a logarithmic law, respectively; while it is contradictory to the observation by Nikora *et al.* [18] [19], who reported a linear $\langle u^+ \rangle$-distribution for $z \leq z_c$.

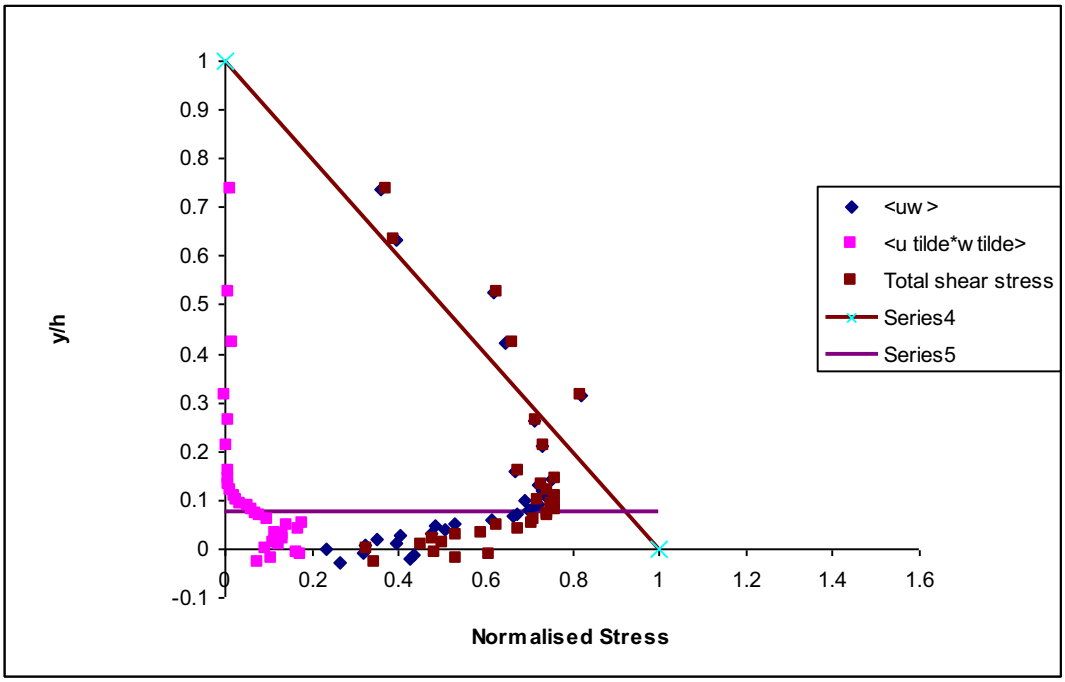

Fig 10: Vertical distributions of normalized SA shear stresses

The momentum balance Manes *et al.*, [results in the SA total shear stress $\langle \tau_t \rangle$, which is obtained by the addition of the SA Reynolds shear stress $\langle \tau_{uw} \rangle$ (= $-\rho \langle \overline{u'w'} \rangle$), form-induced shear stress $\langle \tau_f \rangle$ (= $-\rho \langle \tilde{u}\tilde{w} \rangle$) (Nikora *et al.*, 2007b)]. The total shear stress $\langle \tau_t \rangle$ is balanced by the gravity having a linear distribution given by $\langle \tau_t \rangle / \tau_0 = 1 - \hat{z}$, in which $\hat{z} = z/h$. The vertical

distributions of $\langle \tau_t \rangle$, $\langle \tau_{uw} \rangle$ and $\langle \tau_f \rangle$ shown in Figure 10 in normalized form as $\langle \hat{\tau}_t \rangle$ [= $\langle \tau_t \rangle/(\rho u_*^2)$], $\langle \hat{\tau}_{uw} \rangle$ (= $-\langle \overline{u'w'} \rangle/u_*^2$), $\langle \hat{\tau}_f \rangle$ (= $-\langle \tilde{u}\tilde{w} \rangle/u_*^2$. The Reynolds shear stress $\langle \hat{\tau}_{uw} \rangle$ is the main governing stress across the flow depth with a damping in the vicinity of the gravel-bed due to decrease in turbulence level (u' and w'). This flow zone above the bed, where the damping occurs, is known as form-induced sub-layer that has a thickness of approximately a unit of gravel or $2.5k_s$.

This definition of form-induced sub-layer seems to be more convenient to determine, while other researchers considered the sub-layer at the height at which the $\langle u^+ \rangle$-distribution no longer holds the logarithmic law or at which the $\langle \tau_f \rangle$ attains a threshold value or becomes insignificant [5] [6]. The rise of the form-induced stress, as the time-averaged flow close to the top of the interfacial sub-layer is highly non-homogeneous in space, compensates the damping within the form-induced sub-layer ($0.2 > \hat{z} > \hat{z}_c$, in which $\hat{z}_c = z_c/h$). Therefore, the deviation of $\langle \hat{\tau}_t \rangle$ from the linear gravity profile in form-induced sub-layer is caused primarily by the damping of $\langle \hat{\tau}_{uw} \rangle$, which may be interpreted as the form-induced fluctuations due to the influence of local conditions. This feature was also apparent in previous studies [16] [17]. Within the interfacial sub-layer ($\hat{z} \leq \hat{z}_c$), fluid momentum also gets transferred to the gravels having a decelerating effect on the fluid. In this region, the time-averaged flow is very non-homogeneous, and in general, a gradual damping of $\langle \hat{\tau}_{uw} \rangle$ with a decrease in $\hat{z}$ is evident. However, the data plots for $\hat{z} \rightarrow 0$ and $\hat{z} < 0$ show a drastic diminution of $\langle \hat{\tau}_{uw} \rangle$ that is resulted from invariance characteristic of $\langle u^+ \rangle$-distribution in this flow zone. The form-induced shear stress $\langle \hat{\tau}_f \rangle$ is considerable for $\hat{z} \leq \hat{z}_c$. They gradually increase with a decrease in $\hat{z}$ giving rise to the deceleration in fluid motion. The total shear stress $\langle \hat{\tau}_t \rangle$ (= $\langle \hat{\tau}_{uw} \rangle$ + $\langle \hat{\tau}_f \rangle$) reasonably follows the linear law of the gravity.

5. Conclusion

The findings of the study are concluded as follows. In the experiment the random field approach for gravel-bed roughness characterization appears to be near Gaussian. The distribution of the spatially-averaged streamwise velocity above the roughness crest follows the logarithmic-law. The form-induced stress is mainly effective within the interfacial sub-layer. The local flow characterization shows the presence of three classes of velocity profiles, called S-shaped, accelerated and log classes. It was shown that the local velocity profiles for the S-shape class exhibit an inflectional trend typical of mixing layers. The profiles of the S-shape class were found to be located in the wakes downstream of macro-roughness elements. For the log class profile the mean streamwise velocity fits a logarithmic curve over almost the entire measured profile.

6. References

1. Aberle, J., Koll, K., and Dittrich, A. (2008). “Form induced stresses over rough gravel-beds.” *Acta Geophys*., 56(3), 584-600.
2. Dey, S. (1999). “Sediment threshold.” *Appl. Math. Modelling*, 23(5), 399-417.
3. Dey, S., Dey Sarker, H. K. and Debnath, K. (1999). “Sediment threshold under stream flow on horizontal and sloping beds.” *J. Eng. Mech.*, 125(5), 545-553.

4. Dey, S., Nath, T. K., and Bose, S. K. (2010). "Submerged wall jets subjected to injection and suction from the wall. *J. Fluid Mech.*, 653, 57-97.

5. Dey, S., and Raikar, R.V. (2007). "Characteristics of loose rough boundary streams at near-threshold." *J. Hydraul. Eng.*, 133(3), 288-304.

6. Dey, S., and Sarkar, A. (2008). "Characteristics of turbulent flow in submerged jumps on rough beds." *J. Eng. Mech.*, 134(1), 49-59.

7. Finnigan, J. J. (2000). "Turbulence in plant canopies." *Annu. Rev. Fluid Mech.*, 32, 519-571.

8. Franca, M. J., Czernuszenko, W. (2006). "Equivalent velocity profile for turbulent flows over gravel riverbeds." *Proc. River Flow 2006*, Lisbon, Portugal.

9. Gimenez-Curto, L. A., and Corniero Lera, M. A. (2003). "Highest natural bed forms." *J. Geophys. Res.*, 108(C2), 3046.

10. López, F., and Garcia, M. H. (1998). "Open-channel flow through simulated vegetation: Suspended sediment transport modelling." *Water Resour. Res.*, 34(9), 2341-2352.

11. Manes, C., Pokrajac, D., and McEwan, I. (2007). "Double-averaged open-channel flows with small relative submergence." *J. Hydraul. Eng.*, 133(8), 896-904.

12. Mignot, E., Barthelemy, E., and Hurther, D. (2009a). "Double-averaging analysis and local flow characterization of near-bed turbulence in gravel-bed channel flows." *J. Fluid Mech.*, 618, 279-303.

13. Mignot, E., Hurther, D., and Barthelemy, E. (2009b). "On the structure of shear stress and turbulent kinetic energy flux across the roughness layer of a gravel-bed channel flow." *J. Fluid Mech.*, 638, 423-452.

14.Nikora, Goring, D., and Biggs, B.J.F (1998) "On gravel-bed roughness characterisation."*Water Resour. Res.*, 34(3), 517-527.

15. Nikora, V., and Goring, D. (2000). "Flow turbulence over fixed and weakly mobile gravel beds." *J. Hydraul. Eng.*, 126(9), 679-690.

16. Nikora, V., Goring, D., McEwan, I. and Griffiths, G. (2001). "Spatially averaged open-channel flow over rough bed." *J. Hydraul. Eng.*, 127(2), 123-133.

17. Nikora, V., Koll, K., McEwan, I., McLean, S., and Dittrich, A. (2004). "Velocity distribution in the roughness layer of rough-bed flows." *J. Hydraul. Eng.*, 103(10), 1036-1042.

18. Nikora, V., McEwan, I. K., McLean, S. R., Coleman, S. E., Pokrajac, D., and Walters, R. (2007a). "Double-averaging concept for rough-bed open-channel and overland flows: Theoretical background." *J. Hydraul. Eng.*, 133(8), 873-883.

19. Nikora, V., McLean, S., Coleman, S., Pokrajac, D., McEwan, I., Campbell, L., Aberie, J., Clunie, D., Koll, K. (2007b). "Double-averaging concept for rough-bed open-channel and overland flows: Applications." *J. Hydraul. Eng.*, 133(8), 884-895.

20. Raupach, M. R., Antonia, R. A., and Rajagopalan, S. (1991). "Rough-wall turbulent boundary layers." *Appl. Mech. Rev.*, 44(1), 1-25.

21. Raupach, M. R., and Shaw, R. H. (1982). "Averaging procedures for flow within vegetation canopies." *Boundary-Layer Meteorol.*, 22(1), 79-90.

22. Rodriguez, J. F., Garcia, M. H. (2008). Laboratory measurements of 3-D flow patterns and turbulence in straight open channel with rough bed. *J. Hydraul. Res.*, 46(4), 454-465.

23. Smith, J. D., and McLean, S. R. (1977). Spatially averaged flow over a wavy surface. *J. Geophys. Res.* 83(12), 1735-1746.

24. Wilson, N. R., and Shaw, R. H. (1977). "A higher order closure model for canopy flow." *J. Appl. Meteorol.*, 16(11), 1197-1205.